sustainability

MDPI

Article

Synergistic Effects of Steel Fiber and Rubber Powder on the Physico-Mechanical Properties of UHPC

Changqing Luo [1], Hao Wang [2], Dongbo Cai [1], Anni Wang [2], Lianzhen Zhang [2,*], Deming Wang [3], Chao Wang [1], Degao Kong [1], Sining Huang [2] and Chaohui Xu [1]

[1] The Seventh Engineering Co., Ltd. of CCCC First Highway Engineering Co., Ltd., Zhengzhou 451452, China; 13012447161@163.com (C.L.); 15583130944@163.com (D.C.); 18706567102@163.com (C.W.); 15079316585@163.com (D.K.); wanghuiyu_cumt@163.com (C.X.)

[2] College of Pipeline and Civil Engineering, China University of Petroleum (East China), Qingdao 266580, China; 18663670776@163.com (H.W.); 13396421059@163.com (A.W.); huangsining@upc.edu.cn (S.H.)

[3] School of Transportation and Civil Engineering, Shandong Jiaotong University, Jinan 250357, China; 204116@sdjtu.edu.cn

* Correspondence: zhanglianzhen@upc.edu.cn; Tel.: +86-18265328519

Abstract

This study investigates the synergistic effects of steel fibers and waste rubber powder on the properties of ultra-high-performance concrete (UHPC) to advance its sustainable development. A comprehensive experimental program was conducted, incorporating three types of steel fibers (8 mm straight, and 14 mm and 20 mm hook-end) at volumes up to 2.5%, and rubber powder as quartz sand replacement at levels from 5% to 30%. The flowability, compressive strength, splitting tensile strength, abrasion resistance, and chloride ion penetration resistance of the mixtures were evaluated. The results indicate that steel fiber reinforcement significantly enhances the mechanical and durability properties. Specifically, a 2.5% steel fiber content increased the compressive strength, splitting tensile strength, and abrasion resistance by 28.9%, 55.3%, and 72.4%, respectively. Conversely, the incorporation of rubber powder improved flowability (optimal at 10% replacement) and abrasion resistance (increased by 41.1% at 30% content) but at the expense of reduced mechanical strength and increased chloride ion permeability. The primary novelty of this work lies in systematically quantifying the trade-offs and synergistic interactions between a wide range of steel fiber geometries and high-volume rubber powder content, providing a practical basis for designing UHPC with balanced performance and enhanced sustainability.

Keywords: UHPC; rubber; steel fiber; mechanical characteristic; long-term durability

Check for updates

Academic Editor: Giovanni De Feo

Received: 4 November 2025
Revised: 31 December 2025
Accepted: 7 January 2026
Published: 14 January 2026

Copyright: © 2026 by the authors. Licensee MDPI, Basel, Switzerland. This article is an open access article distributed under the terms and conditions of the Creative Commons Attribution (CC BY) license.

1. Introduction

As a multifunctional material, concrete is renowned for its durability and performance in harsh environments [1–3]. The development of ultra-high-performance concrete (UHPC) has further pushed the boundaries of cement-based materials [4–8], offering exceptional strength, ductility, and durability [9–12]. Over the past decades, research has focused on enhancing UHPC's properties and sustainability by incorporating various supplementary materials, such as fly ash and silica fume [13–17].

The use of recycled materials is a key pathway towards sustainable construction. Recycled rubber powder from end-of-life tires has gained attention for its potential to improve concrete's impact resistance and energy absorption [18,19]. However, its incorporation often leads to a significant reduction in compressive strength, as noted by Pham et al. [20],

who observed a 50.2% strength loss in UHPC with 40% rubber content. To mitigate this strength loss while retaining benefits, steel fibers are frequently introduced. They are highly effective in enhancing the tensile strength and toughness of concrete [21]. Studies like that of Chen et al. [22] have confirmed that steel fibers can partially compensate for the strength reduction caused by rubber powder in UHPC.

Despite these investigations, critical gaps remain in the existing literature. First, most studies on rubberized UHPC focus on fine-grained matrices without coarse aggregate. Our previous research has demonstrated that incorporating coarse aggregate is a viable strategy for reducing the cost of UHPC [23]. Building upon that foundation, this study specifically investigates the performance of UHPC with coarse aggregate modified with rubber powder and steel fibers, a system less explored. Second, while the individual effects of rubber powder or steel fibers are documented, a systematic analysis of their synergistic effects—particularly on long-term durability and abrasion resistance in a system of UHPC with coarse aggregate—is lacking. The optimal combination for balancing mechanical properties, durability, and flowability in such a sustainable matrix is not well-defined.

Therefore, this paper presents a comprehensive experimental investigation into the synergistic effects of steel fiber type (8 mm straight and 14 mm and 20 mm hook-end), fiber content (0–2.5%), and rubber powder content (0–30% sand replacement) on the fresh, mechanical, and durability properties of UHPC with coarse aggregate. The properties evaluated include flowability, compressive strength, splitting tensile strength, abrasion resistance, and chloride ion penetration resistance. The novelty of this work lies in (1) extending the study of rubber–steel fiber synergy to a more practical and economical UHPC with a coarse aggregate system, and (2) providing a complete performance map that quantifies trade-offs and synergies to guide the design of sustainable UHPC with balanced properties. The findings are expected to offer valuable insights for practical applications that require enhanced durability and abrasion resistance, such as pavements and marine structures.

2. Materials and Methods

2.1. Raw Materials

Portland cement (PII 42.5R), silica fume, fly ash, quartz sand, coarse aggregates, and water were the basic materials for preparing the UHPC. Rubber powder, steel fibers, and polycarboxylate superplasticizer serve as the additional materials for preparing the UHPC. The chemical compositions of cement, silica fume, and fly ash are, respectively, shown in Tables 1–3. The particle size distributions of cement, quartz sand, silica fume, and fly ash are displayed in Figure 1. Granite served as the coarse aggregate [24], and the particle size range was 5–10 mm. The physical characteristics of coarse aggregate are shown in Table 4. The steel fiber is shown in Figure 2, using 8 mm straight, 14 mm hook-end, and 20 mm hook-end copperplated steel fibers [25]. The physical characteristics of steel fibers are shown in Table 5. The rubber powder was the particle obtained from the crushing of waste tires, with an irregular shape and typical tearing texture on the surface (shown in Figure 3). The particle size distribution range of rubber powder measured by the standard screening method was 0.38–0.83 mm, its D50 was 0.62 mm, and the apparent density was 1.01×10^3 kg/m^3.

Table 1. Chemical composition of Portland cement (PII 42.5R) (wt.%).

CaO	SiO_2	Fe_2O_3	MgO	Ti_2O_3	Al_2O_3	K_2O	Rest
64.48	21.4	3.5	1.46	0.58	5.45	0.80	2.33

Table 2. Chemical composition of silica fume (wt.%).

CaO	SiO_2	MgO	Al_2O_3	K_2O	Na_2O	P_2O_5	Rest
0.37	95.12	0.42	0.23	0.86	0.13	2.0	0.87

Table 3. Chemical composition of fly ash (wt.%).

CaO	SiO_2	Fe_2O_3	MgO	TiO_2	Al_2O_3	K_2O	Na_2O	SO_3	Rest
12.41	49.55	4.35	1.54	1.09	24.55	0.95	0.19	0.91	4.46

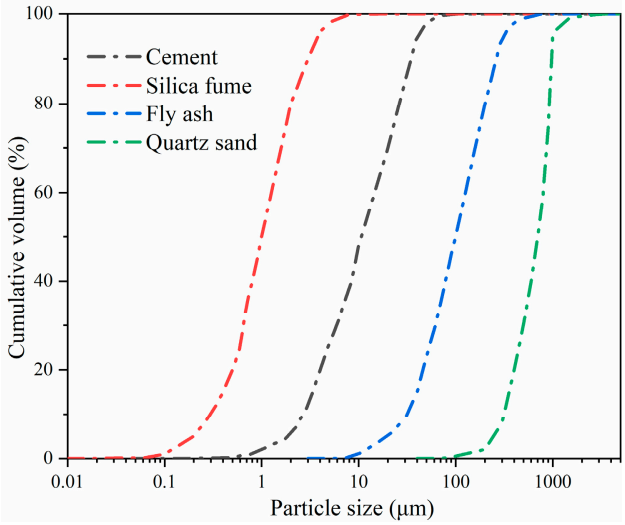


Figure 1. The particle size distributions of materials.

Table 4. Physical properties of granite coarse aggregate.

Water Absorption	Hardness	Roughness	Unconfined Compressive Strength (MPa)	Brazilian Splitting Strength (MPa)	Angularity
12.41	49.55	4.35	1.54	1.09	24.55

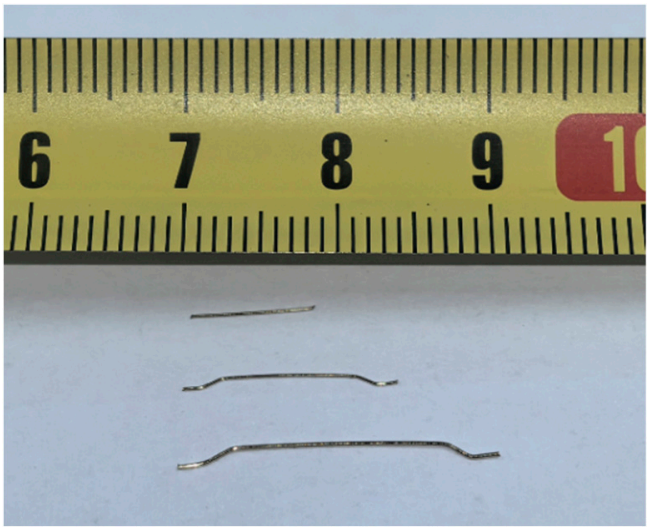


Figure 2. Steel fibers.

Table 5. Physical characteristics of steel fibers.

Steel Fiber	Length/mm	Shape	Tensile Strength/MPa	Equivalent Diameter/mm	Length–Diameter Ratio
Type-1	8	Straight	2700	0.145	55
Type-2	14	Hook-end	2550	0.22	65
Type-3	20	Hook-end	2550	0.30	65



Figure 3. Rubber powder.

2.2. Experiment Design and Mixing Procedure

Based on the principles of existing mix design theories [2,26,27], the UHPC matrix was formulated with a cementitious system comprising cement, fly ash, and silica fume in the mass ratio of 7:2:1. A constant quartz sand-to-cementitious mass ratio of 1.0 was maintained. The polycarboxylate superplasticizer dosage was fixed at 2% of the total cementitious mass, and the water-to-binder ratio (W/B) was set at 0.16.

The influence of steel fiber type and content, as well as rubber powder content, on the performance of UHPC was investigated. The rubber powder replaced quartz sand (later expressed as rubber powder content) with a range from 0 to 30% in UHPC. The steel fiber content ranged from 0% to 2.5% of the total material mass, and the types were 8 mm straight, 14 mm hook-end, and 20 mm hook-end steel fibers. The mix proportions for these content levels are shown in Table 6.

Cement, fly ash, silica fume, coarse aggregate, rubber powder, and quartz sand were added to the mixer and stirred slowly for 2 min, and then water and polycarboxylate superplasticizer were added to the mixer and stirred quickly for 5 min. After waiting for the mixing in the mixer to be uniform and have sufficient viscosity, the steel fiber was added and stirred for 8 min. After stirring, the slump flow and slump were conducted according to ASTM C143 [28] and ASTM C1611 [29]. The freshly mixed UHPC was first cast into molds. The molds were subsequently wrapped in plastic film to retain moisture, then cured indoors at 20 ± 2 °C for 48 h before demolding. Following demolding, all specimens were transferred to a controlled curing environment (20 ± 2 °C and >95% relative humidity) for a standard 28-day period.

Table 6. Mix proportion (kg/m^3).

Samples	Coarse Aggregate	Cement	Silica Fume	Fly Ash	Water	PS	Steel Fiber	Steel Fiber Type	Quartz Sand	Rubber Powder
0Ru-0St	600	610.09	87.16	174.31	139.45	17.43	/	/	871.56	0
5Ru-0St	600	610.09	87.16	174.31	139.45	17.43	/	/	827.98	43.578
10Ru-0St	600	610.09	87.16	174.31	139.45	17.43	/	/	784.40	87.156
15Ru-0St	600	610.09	87.16	174.31	139.45	17.43	/	/	740.83	130.73
20Ru-0St	600	610.09	87.16	174.31	139.45	17.43	/	/	697.25	174.31
30Ru-0St	600	610.09	87.16	174.31	139.45	17.43	/	/	610.09	261.46
0Ru-0.5St14	600	597.49	85.36	170.71	136.57	17.07	39.25	14 mm	853.55	/
0Ru-1St14	600	584.89	83.56	167.11	133.69	16.71	78.5	14 mm	835.55	/
0Ru-1.5St14	600	572.28	81.75	163.51	130.81	16.35	117.75	14 mm	817.54	/
0Ru-2St14	600	559.68	79.95	159.91	127.93	15.99	157	14 mm	799.54	/
0Ru-2.5St14	600	547.05	78.15	156.3	125.04	15.63	196.25	14 mm	781.5	/
0Ru-2St8	600	559.68	79.95	159.91	127.93	15.99	157	8 mm	799.54	/
0Ru-2St20	600	559.68	79.95	159.91	127.93	15.99	157	20 mm	799.54	/
5Ru-2St14	600	559.68	79.95	159.91	127.93	15.99	157	14 mm	759.56	39.98
10Ru-2St14	600	559.68	79.95	159.91	127.93	15.99	157	14 mm	719.59	79.95
15Ru-2St14	600	559.68	79.95	159.91	127.93	15.99	157	14 mm	679.61	119.93
20Ru-2St14	600	559.68	79.95	159.91	127.93	15.99	157	14 mm	639.63	159.91
30Ru-2St14	600	559.68	79.95	159.91	127.93	15.99	157	14 mm	559.68	239.86

2.3. Test Methods

Standard test methods were employed to evaluate both the strength and long-term durability performance of the UHPC. Compressive and splitting tensile strength were tested based on the ASTM C39/C39M-21 [30] and ASTM C496/C496M-17 [31], respectively. Three parallel specimens were prepared and tested in each test group to ensure the repeatability of the results. For the compression test, 100 mm cubes were loaded at a rate of 1.2–1.4 MPa/s until failure. The tensile strength test employed 150 mm cubes subjected to a constant loading rate of 0.12 MPa/s.

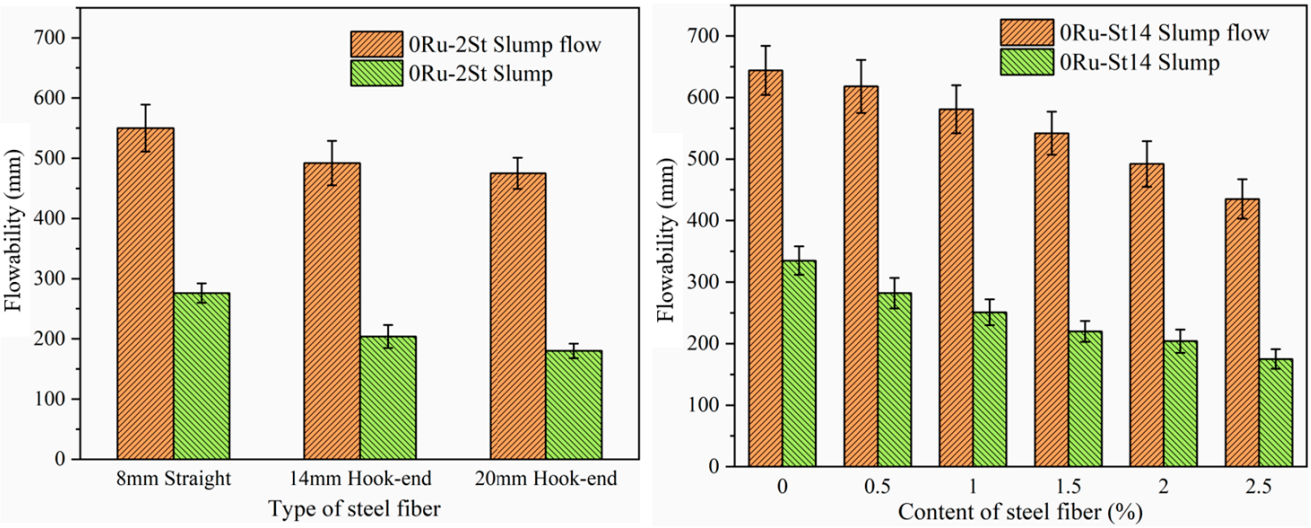
Considering the potential application of UHPC in marine structures (such as port facilities and bridge piers), its resistance to chloride ion penetration and abrasion was critically evaluated. The chloride diffusion coefficient was determined using the Rapid Chloride Migration (RCM) method per NT Build 492 [32] on Ø100 × 50 mm disks that were saturated after standard 28-day curing. Three parallel specimens were tested for each mix ratio. Abrasion resistance, a property enhanced by steel fiber and rubber powder, was tested according to ASTM C779/C779M-09 [33]. This involved subjecting a Ø300 × 100 mm cylindrical sample to a 72 h underwater abrasion process using 70 rotating steel balls of varying sizes (12.7, 19.1, and 25.4 mm) at 1200 rpm. The mass loss of the sample, pre-saturated for 48 h, was measured after the test. Three parallel specimens were also tested for each mix ratio.

3. Results

3.1. Flowability

Figure 4 shows the influence of steel fiber type and content on the flowability of UHPC. The slump flow and slump of UHPC mixed with 8 mm straight steel fiber are 11.8% and 35.3% higher than those mixed with 14 mm hook-end steel fiber, and 15.8% and 53.3% higher than those mixed with 20 mm hook-end steel fiber. From a materials perspective, the superior flowability of mixtures with short and straight fibers stems from their lower aspect ratio (length–diameter ratio = 55) and minimal geometric obstruction. The smooth surface and absence of hooks reduce inter-fiber friction and allow easier rotation within the paste, thereby lowering viscosity. Conversely, the hook-end fibers (length–diameter

ratio = 65) generate significant mechanical interlocking due to their deformed geometry, creating localized resistance points that impede slurry flow [25]. This effect is amplified in longer fibers (20 mm), which exhibit greater contact area with the matrix and increased probability of entanglement.



(**a**) Type of steel fiber (**b**) Content of steel fiber

Figure 4. Influence of steel fiber type and content on flowability of UHPC.

As the steel fiber content increases from 0 to 2.5%, the slump flow of UHPC drops by 32.5%, while its slump declines by 47.8%. Beyond 1.5% volume fraction, fibers form a connected network that acts as a rigid skeleton, trapping aggregates and paste within its structure. This network increases yield stress and plastic viscosity by physically obstructing particle movement and absorbing free water via hydrophilic surface interactions, reducing lubricating films between particles [34]. The agglomeration observed around aggregates further exacerbates this by creating zones of high fiber density that act as flow barriers.

Figure 5 shows the influence of steel fiber type and content on flowability of UHPC. As the content of rubber powder increases, the flowability of UHPC first rises and then falls. Notably, the UHPC with 10% rubber powder content exhibits the highest flowability. Compared with UHPC without rubber powder, the slump flow is increased by 21.9%, and the slump is increased by 34.9%. When the rubber powder content reaches 30%, the slump flow is decreased by 13.9%, and the slump is decreased by 40.6%. The nonmonotonic trend in flowability is governed by competing mechanisms: At low contents ($\leq$10%), rubber powders act as "ball bearings" due to their smooth hydrophobic surfaces and low elastic modulus. They reduce interparticle friction by separating rigid aggregates (granite, quartz sand) and sliding at contact points, enhancing lubricity. This effect peaks at 10% replacement, where particle spacing optimizes lubrication without significantly increasing surface area demand. However, rubber powder possesses a comparatively large specific surface area. Once its content increases beyond 10%, more concrete slurry becomes necessary to cover its surface, and this subsequently obstructs the flow of the concrete slurry.

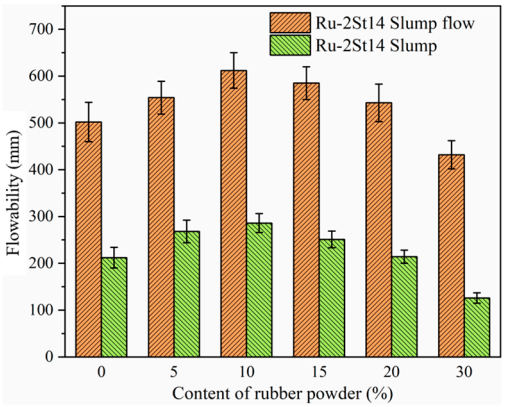
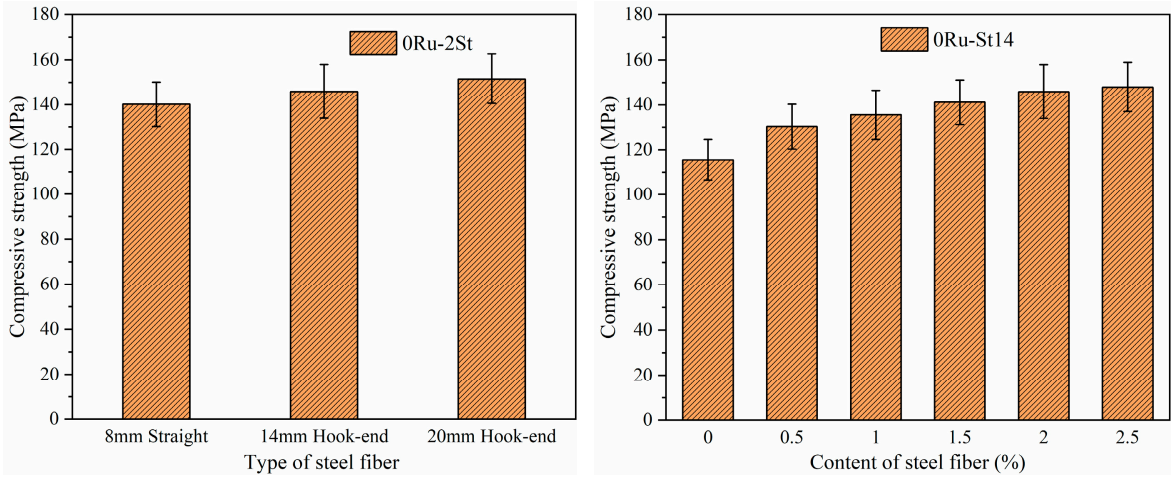


Figure 5. Influence of rubber powder content on flowability of UHPC.

3.2. Compressive Strength

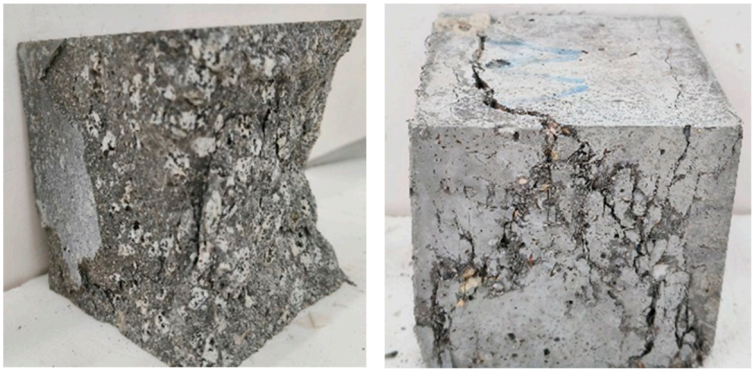
Figure 6 shows the influence of steel fiber type and content on the compressive strength of UHPC. Under the scenario of 2% steel fiber content, UHPC with 8 mm steel fibers has a compressive strength of 140.18 MPa, UHPC with 14 mm steel fibers has a compressive strength of 145.97 MPa, and UHPC with 20 mm steel fibers has a compressive strength of 151.62 MPa. It may be concluded that the steel fiber type exerts little influence on the compressive strength of UHPC. However, longer hook-end fibers (e.g., 20 mm) provide superior crack-bridging efficiency due to enhanced mechanical anchorage at the fiber–matrix interface. The hooked ends restrict fiber pullout during loading, promoting stress redistribution and delaying microcrack coalescence. This interfacial locking effect compensates for the weak zones in the matrix, leading to marginally higher compressive strength.



(**a**) Type of steel fiber (**b**) Content of steel fiber

Figure 6. UHPC Influence of steel fiber type and content on compressive strength of UHPC.

As the content of steel fibers increases from 0% to 2.5%, the compressive strength of UHPC rises from 115.32 MPa to 148.62 MPa, representing an increase of 28.9%. In the UHPC system, steel fiber, coarse aggregate, and UHPC matrix form a stable three-dimensional skeleton system to bear the external load together. When subjected to external pressure, the steel fiber in the UHPC system acts as a 'reinforcing bar', which effectively disperses stress, reduces stress concentration, and limits the generation and development of microcracks, as shown in Figure 7, thus improving compressive strength.



(**a**) 0% steel fiber (**b**) 2% steel fiber

Figure 7. Compression failure pattern of UHPC.

Figure 8 shows the influence of rubber powder content on compressive strength of UHPC. As rubber powder content increases, the compressive strength of UHPC drops. The compressive strength of UHPC with 0% rubber powder is 145.97 MPa, and when the rubber powder content gradually goes up to 30%, the compressive strength of UHPC experiences a linear decrease of 38.1%. Compared with quartz sand, rubber powder is soft, and it is more likely to produce internal deformation when subjected to external force in UHPC, which is not conducive to compression. At the same time, rubber powder, as an organic polymer material, is unable to chemically combine with cementitious materials when compared with traditional aggregates. This results in insufficient adhesion between the concrete matrix and rubber powder, thus leading to a drop in the compressive strength of UHPC.

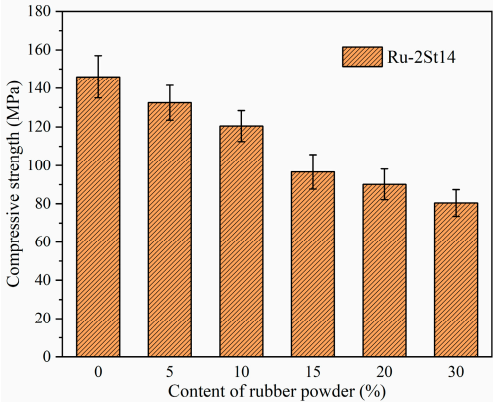
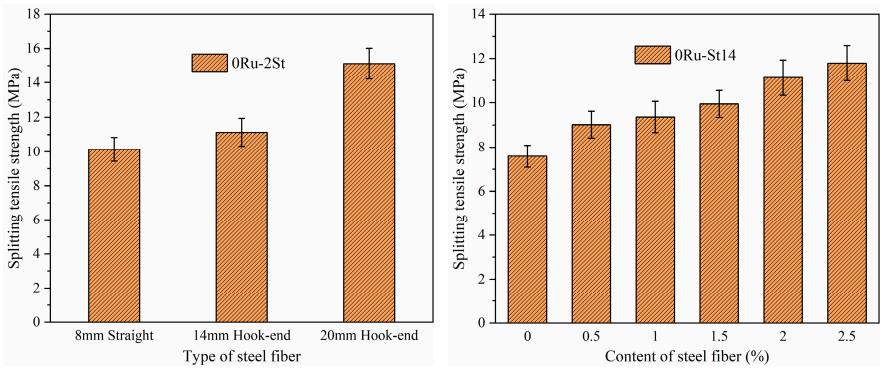


Figure 8. Influence of rubber powder content on compressive strength of UHPC.

3.3. Splitting Tensile Strength

Figure 9 shows the influence of steel fiber type and content on the splitting tensile strength of UHPC. The type of steel fiber serves as an important factor affecting the splitting tensile strength of UHPC. The splitting tensile strength of UHPC devoid of steel fibers is 7.59 MPa; relative to this, the splitting tensile strength of UHPC containing 8 mm, 14 mm, and 20 mm steel fibers rose by 33.6%, 46.6%, and 99.2%, respectively. Hook-end fibers (14 mm and 20 mm) significantly outperform straight fibers due to their mechanical interlock with the matrix. The hooks resist pullout forces during tensile loading, enabling efficient stress transfer across cracks. Longer fibers (20 mm) bridge wider cracks, dissipating energy through extended debonding and frictional pullout processes, thus substantially enhancing post-cracking ductility.



(**a**) Type of steel fiber (**b**) Content of steel fiber

Figure 9. Influence of steel fiber type and content on splitting tensile strength of UHPC.

The incorporation of steel fiber has a significant effect on the splitting tensile strength of UHPC. With the increase in steel fiber content from 0.5% to 2.5%, the splitting tensile strength of UHPC increases by 18.7% to 55.3% compared with that without steel fiber. When the samples are subjected to splitting tension, the steel fiber plays a bridge-like role in the UHPC matrix, effectively connecting and preventing the development of cracks and transmitting the tensile stress to other steel fibers through the 'bridging effect'. Therefore, the more steel fiber content, the stronger the splitting tensile strength.

Steel fiber incorporation has a significant effect on the splitting tensile strength of UHPC. With the steel fiber content increasing from 0.5% to 2.5%, the splitting tensile strength of UHPC increases by 18.7% to 55.3% compared with that of UHPC without steel fibers. When the samples are exposed to splitting tension, steel fibers play a bridge-like role in the UHPC matrix: they effectively join different parts of the matrix, stop cracks from growing, and transmit tensile stress to other steel fibers through the "bridging effect." Therefore, the more steel fibers are added (i.e., higher content), the stronger the splitting tensile strength becomes.

Figure 10 shows the influence of rubber powder content on the splitting tensile strength of UHPC. The impact of rubber powder on the splitting tensile strength of UHPC is insignificant prior to a content of 20%. With the rubber powder content increasing to 30%, the splitting tensile strength of UHPC falls to 10.41 MPa, showing a 6.4% decrease compared to rubber-powder-free UHPC. When rubber content is high (>20%), the percolation of weak rubber–cement ITZs takes the lead in governing the failure of UHPC. Rubber powder acts as voids under tension, reducing load-bearing cross-sections and facilitating crack propagation along ITZ networks. Although rubber's elasticity might mitigate brittle failure, its poor adhesion to the matrix outweighs this benefit in tensile loading scenarios.

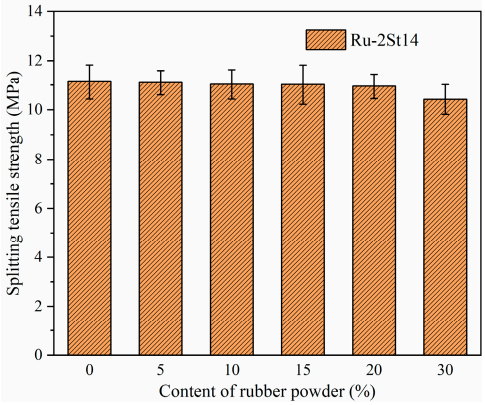
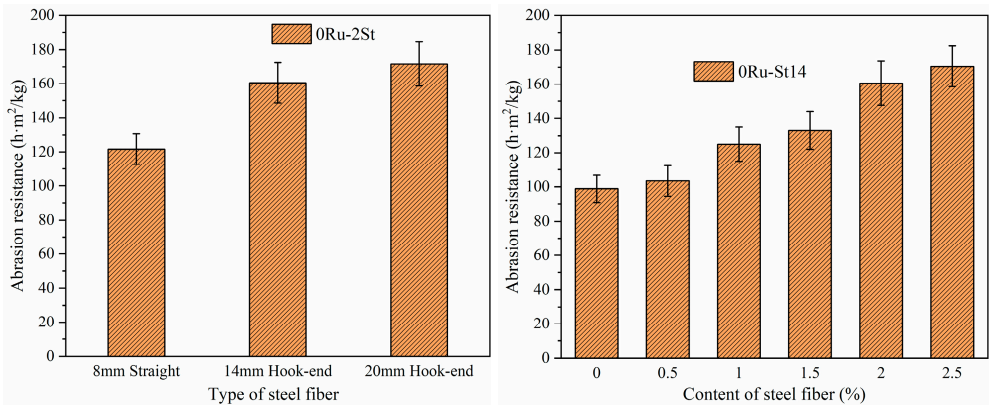


Figure 10. Influence of rubber powder content on splitting tensile strength of UHPC.

3.4. Abrasion Resistance

Figure 11 shows the influence of steel fiber type and content on the abrasion resistance of UHPC. As the length of steel fibers increases, the abrasion resistance of UHPC rises gradually. Specifically, the abrasion resistance of UHPC mixed with 8 mm, 14 mm, and 20 mm steel fibers is 23.12%, 62.5%, and 73.7% higher than that of UHPC without any steel fibers, respectively. Longer hook-end fibers form a robust 3D network that physically shields the matrix. When surface abrasion exposes fibers, their anchorage resists dislodgement, while friction between fibers and abrasive media dissipates kinetic energy. The hooked ends further enhance fiber retention, maintaining structural integrity even after matrix erosion.



(**a**) Type of steel fiber (**b**) Content of steel fiber

Figure 11. Influence of steel fiber type and content on abrasion resistance of UHPC.

As the content of steel fiber increases, the abrasion resistance of UHPC shows a gradual upward trend. Specifically, when steel fiber content increases from 0% to 2.5%, the abrasion resistance of UHPC goes from 98.81 h·m^2/kg to 170.42 h·m^2/kg, corresponding to a 72.4% increase. Following the incorporation of steel fiber into UHPC, the steel fibers and concrete matrix jointly create a three-dimensional steel fiber network. The robust physical friction resistance of this network, along with the bonding force between the fibers and the concrete matrix, functions collaboratively to impart toughness to UHPC. After the UHPC surface concrete matrix is scoured, the steel fibers distributed between the microcracks will slightly expose the surface of the concrete matrix (shown in Figure 12). Part of the kinetic energy of the sand-carrying water flow is consumed during the friction process of the steel fiber, thus preventing the expansion of the microcracks on the surface of the UHPC samples.



(**a**) 0% steel fiber (**b**) 2% steel fiber

Figure 12. Abrasion morphology of UHPC.

Figure 13 shows the influence of rubber powder content on abrasion resistance. Abrasion morphology of UHPC with 30% rubber powder is shown in Figure 14. As the content

of rubber powder increases gradually, the abrasion resistance of UHPC also improves step by step. The abrasion resistance of UHPC without any rubber powder added is 160.57 h·m^2/kg; when the rubber powder content reaches 30%, this resistance of UHPC rises to 226.53 h·m^2/kg, which is equivalent to an increase of 41.1%. Rubber powder absorbs the impact energy via elastic deformation and reduces cutting damage. Their viscoelasticity dissipates stress waves generated during collisions, protecting the brittle cement matrix. However, at high content (>20%), weak ITZs may compromise this benefit by promoting rubber particle dislodgement.

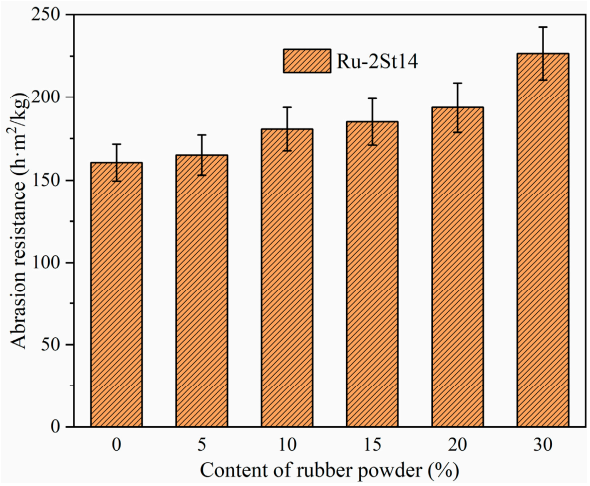


Figure 13. Influence of rubber powder content on abrasion resistance.

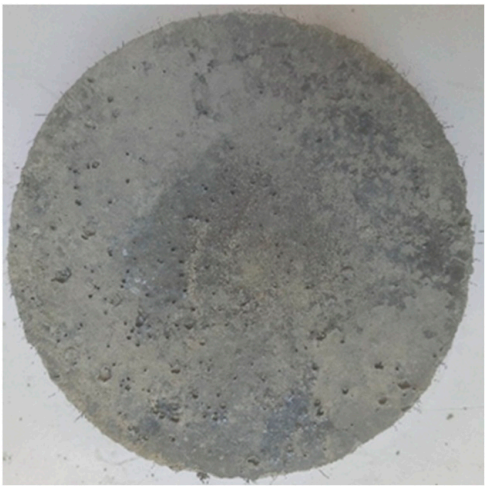


Figure 14. Abrasion morphology of UHPC with 30% rubber powder.

3.5. Chloride Ion Penetration Resistance

Figure 15 shows the influence of rubber powder content on chloride ion penetration resistance. The chloride ion penetration resistance decreases with the increase in rubber powder content. The chloride diffusion coefficient of UHPC without rubber powder is 3.86×10^{-13} m^2/s, and that with 30% rubber powder is 9.88×10^{-12} m^2/s—25.6 times higher. Hydrophobic rubber powder creates discontinuous ITZs with the cement matrix, forming interconnected microcracks and voids. These percolated pathways act as conduits for chloride ingress. Additionally, rubber powder hinders cement hydration at interfaces, increasing ITZ porosity and accelerating ionic diffusion.

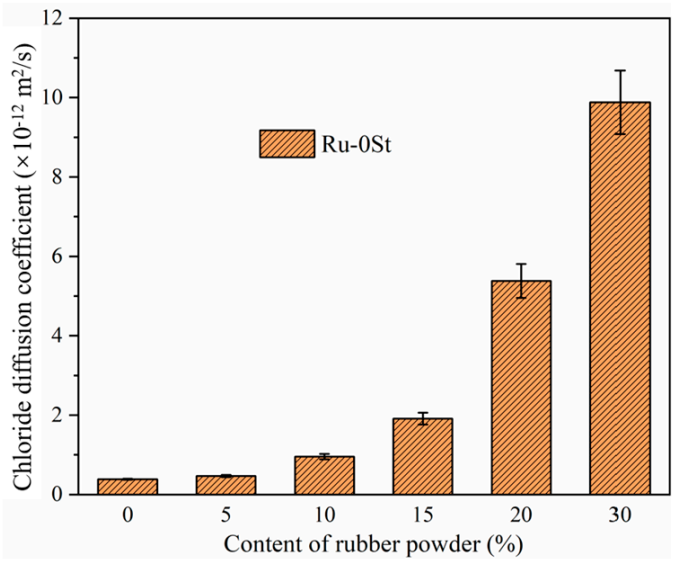


Figure 15. Influence of rubber powder content on chloride ion penetration resistance.

4. Discussion

Steel fibers and rubber powders serve as essential functional components in ultra-high-performance concrete (UHPC). A comprehensive understanding of their individual and interactive mechanisms is crucial for optimizing the mechanical and durability properties of UHPC. This section provides an in-depth analysis of their respective roles and synergistic effects (shown in Figure 16).

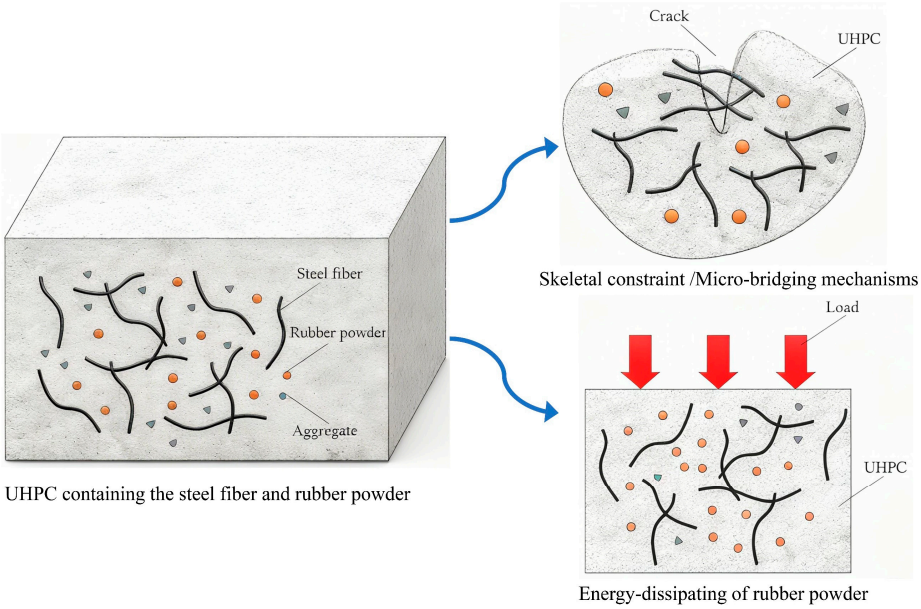


Figure 16. Mechanism of action.

The inclusion of steel fibers substantially modifies the mechanical and durability behavior of UHPC. The consistent improvements in compressive and tensile strength with increasing fiber content are attributed to the well-documented mechanisms of skeletal constraint and crack bridging. More notably, there is a dramatic enhancement in abrasion resistance, reaching up to a 72.4% increase with 2.5% fiber content. Under abrasive actions such as micro-cutting and grinding, the hard steel fibers act as a primary wear-resistant phase, shielding the softer cementitious matrix. Furthermore, the three-dimensional fiber network effectively binds the matrix, mitigating surface spalling and matrix detachment

caused by repeated impact or scratching. The abrasion process likely involves the progressive exposure and eventual pullout of fibers, which itself consumes significant energy, thereby translating the fiber's bridging toughness into improved surface durability.

The effect of rubber powders on UHPC performance, as confirmed in this study, presents a dualistic character. The improvement in flowability (at optimal content) and abrasion resistance is primarily due to the elastic nature of rubber particles, which act as energy-dissipating inclusions under impact or abrasive loads. However, the concomitant reduction in mechanical strength and the increase in chloride ion diffusion coefficient are direct consequences of the weak interfacial transition zone between the hydrophobic rubber and the hydrophilic cement matrix. This porous ITZ compromises the structural integrity and creates pathways for ingress of harmful agents, highlighting a critical trade-off that must be managed in design.

When co-incorporated, steel fibers and rubber powders exhibit a distinct synergy that elevates the overall composite performance, as conceptually illustrated in Figure 16. The key synergy lies in the fiber network's ability to compensate for the weaknesses introduced by the rubber. The three-dimensional steel skeleton physically interlocks with and stabilizes the weak rubber–matrix ITZ, preventing localized defects from coalescing into major cracks under load. This confinement effect is crucial for maintaining long-term durability, as it also blocks the interconnected permeability paths that would otherwise form at high rubber content, thereby explaining the moderated chloride ingress in some hybrid mixes. Conversely, the presence of rubber particles enhances the composite's ability to absorb energy prior to the mobilization of fiber bridging, contributing to the observed toughness. This synergistic mechanism effectively decouples the strength-permeability dependency often seen in rubberized concrete, offering a route to design UHPC with balanced and superior properties.

5. Conclusions

In this paper, the influence of steel fiber types, content, and rubber powder content on the physico-mechanical performance (including flowability, mechanical properties, and long-term durability) of ultra-high-performance concrete (UHPC) was investigated. The flowability, compressive strength, splitting tensile strength, abrasion resistance, and chloride ion penetration resistance of the UHPC specimens incorporated with the steel fibers and rubber powder were explored. The findings of this study will provide valuable insights for the practical application of UHPC in construction, especially in enhancing its sustainability through the recycling of waste rubber. The main findings of this study are as follows:

(1) Steel fibers are pivotal for enhancing mechanical strength and abrasion resistance. The 20 mm hook-end fibers provided the best overall performance due to superior crack-bridging and anchorage. A content of 2.0% to 2.5% was identified as the effective range for maximizing compressive/tensile strength and abrasion resistance (up to 72.4% improvement), beyond which flowability is significantly compromised. Rubber powder improves flowability (peaking at 10% replacement) and abrasion resistance (up to 41.1% increase at 30%) through its elastic and lubricating effects. However, it inevitably reduces mechanical strength and increases chloride permeability. For applications where durability against chloride ingress is critical, its content should be limited, whereas for applications prioritizing abrasion/impact resistance, higher contents (e.g., 20–30%) can be utilized.

(2) The co-incorporation of both materials enables a synergistic design strategy to balance the trade-offs. The three-dimensional steel fiber network can physically confine the weak interfacial zones around rubber particles, suppressing the growth of microc-

racks. An optimized blend of approximately 2% steel fiber (14–20 mm hook-end) with 10–15% rubber powder is recommended. This combination leverages the rubber's flowability and energy-absorption benefits while utilizing the fiber network to maintain robust mechanical strength and mitigate chloride diffusion, offering a practical pathway for designing UHPC with balanced performance.

(3) The developed UHPC with rubber powder and steel fiber shows high potential for sustainable construction in demanding environments, such as heavy-duty pavements, bridge deck overlays, and marine splash zones, where enhanced abrasion resistance, impact tolerance, and a reduced carbon footprint are simultaneously required. Future research should focus on the following: Microscopic validation of the proposed synergistic mechanisms using SEM and MIP to directly observe the fiber–rubber–matrix interactions; long-term field performance and durability monitoring under real environmental conditions; life cycle assessment to quantitatively evaluate the environmental benefits of this sustainable UHPC system; and numerical modeling of its abrasion resistance to facilitate predictive design.

Author Contributions: Conceptualization, C.L. and H.W.; methodology, C.L., D.C. and A.W.; validation, D.W. and C.W.; formal analysis, C.L. and A.W.; investigation, A.W., D.K. and S.H.; resources, L.Z. and C.L.; data curation, C.X.; writing—original draft preparation, C.L. and H.W.; writing—review and editing, D.C. and L.Z.; supervision, L.Z.; project administration, L.Z.; funding acquisition, L.Z. All authors have read and agreed to the published version of the manuscript.

Funding: This work is supported by the National Key Research and Development Program (2022YFB2603000), the National Natural Science Foundation of China (52179120 and 51909270), the Fundamental Research Funds for the Central Universities (23CX07013A), and the Youth Science and Technology Support Program Project of Shandong Province (2023KJ058).

Institutional Review Board Statement: Not applicable.

Informed Consent Statement: Not applicable.

Data Availability Statement: The raw data supporting the conclusions of this article will be made available by the authors on request.

Conflicts of Interest: Authors Changqing Luo, Dongbo Cai, Chao Wang, Degao Kong and Chaohui Xu were employed by the company The Seventh Engineering Co., Ltd. of CCCC First Highway Engineering Co., Ltd. The remaining authors declare that the research was conducted in the absence of any commercial or financial relationships that could be construed as a potential conflict of interest.

References

1. Peng, Y.X.; Yu, L.Y.; Qian, J.Y.; Li, W.; Zhang, T.; Zhou, L.J. Dynamic tensile behavior and crack propagation in coral aggregate seawater shotcrete: Experimental investigation and numerical simulation. *Cem. Concr. Comp.* **2025**, *159*, 106010. [CrossRef]
2. Wang, X.; Zhang, L.; Zhang, Q.; Liu, R.; Huang, C. A stepwise calculation method for grouting penetration in rough rock fracture based on fracture segment division. *Tunn. Undergr. Space Technol.* **2025**, *166*, 106944. [CrossRef]
3. Li, Z.; Lv, S.; Liu, L.; Guo, J.; Liu, T. Compressive Deformation Characteristics of Sintered Loess after Being Saturated with Water. *Int. J. Geomech.* **2024**, *24*, 04024177. [CrossRef]
4. Li, W.; Zhang, Q.S.; Wang, X.C.; Yu, L.Y.; Li, Z.Q. Synergistic effect of particle size, carboxymethyl starch and Na_2CO_3 on rheological and filtration property of bentonite-based material. *Case Stud. Constr. Mater.* **2024**, *21*, e03537. [CrossRef]
5. Li, W.; Yu, L.Y.; Tan, Y.Z.; Wu, L.R.; Qian, J.Y. Mechanical properties and impact behavior of frozen clay: Insights from static mechanical tests, fly-plate tests, and split-Hopkinson pressure bar analysis. *Phys. Fluids* **2024**, *36*, 057138. [CrossRef]
6. Li, Z.; Ma, J.; Liu, X.; Liu, L.; Cai, G.; Peng, L.; Xiong, H. Exploring the temperature, humidity, and deformation characteristics of gravel replacement foundations in seasonally frozen zones: A model testing study. *Bull. Eng. Geol. Environ.* **2025**, *84*, 141. [CrossRef]
7. Richard, P.; Cheyrezy, M. Composition of reactive powder concretes. *Cem. Concr. Res.* **1995**, *25*, 1501–1511. [CrossRef]

8. Richard, P.; Cheyrezy, M. Reactive powder concretes with high ductility and 200–800 MPa compressive strength. *Spec. Publ.* **1994**, *144*, 507–518.
9. Soliman, A.M.; Nehdi, M.L. Effect of partially hydrated cementitious materials and superabsorbent polymer on early-age shrinkage of UHPC. *Constr. Build. Mater.* **2013**, *41*, 270–275. [CrossRef]
10. Wille, K.; Naaman, A.E.; El-Tawil, S.; Parra-Montesinos, G.J. Ultra-high-performance concrete and fiber reinforced concrete: Achieving strength and ductility without heat curing. *Mater. Struct.* **2012**, *45*, 309–324. [CrossRef]
11. Huang, H.; Ye, G. Examining the "time-zero" of autogenous shrinkage in high/ultra-high performance cement pastes. *Cem. Concr. Res.* **2017**, *97*, 107–114. [CrossRef]
12. Alkaysi, M.; El-Tawil, S. Effects of variations in the mix constituents of ultra high performance concrete (UHPC) on cost and performance. *Mater. Struct.* **2016**, *49*, 4185–4200. [CrossRef]
13. Yang, J.; Peng, G.; Gao, Y.; Zhang, H. Mechanical properties and durability of ultra-high performance concrete incorporating coarse aggregate. *Key Eng. Mater.* **2015**, *629*, 96–103. [CrossRef]
14. Li, P.; Yu, Q.; Brouwers, H.J.H. Effect of coarse basalt aggregates on the properties of Ultra-high-Performance Concrete (UHPC). *Constr. Build. Mater.* **2018**, *170*, 649–659. [CrossRef]
15. Haile, B.F.; Jin, D.W.; Yang, B.; Park, S.; Lee, H.K. Multi-level homogenization for the prediction of the mechanical properties of ultra-high-performance concrete. *Constr. Build. Mater.* **2019**, *229*, 116797. [CrossRef]
16. Ming, S.; Terry, B.; Phillip, V. Plastic and early-age shrinkage of Ultra-high-performance concrete (UHPC): Experimental study of the effect of water to binder ratios, silica fume dosages under controlled curing conditions. *Case Stud. Constr. Mater.* **2022**, *16*, e00948.
17. Gesoglu, M.; Güneyisi, E.; Asaad, D.S.; Muhyaddin, G.F. Properties of low binder ultra-high performance cementitious composites: Comparison of nanosilica and microsilica. *Constr. Build. Mater.* **2016**, *102*, 706–713. [CrossRef]
18. Ryu, G.S.; Kang, S.T.; Park, J.J.; Koh, K.T.; Kim, S.W. Evaluation of fundamental UHPC properties according to the shape of steel fiber. *Key Eng. Mater.* **2011**, *452*, 717–720. [CrossRef]
19. Roychand, R.; Gravina, R.; Zhuge, Y.; Ma, X.; Youssf, O.; Mills, J.E. A comprehensive review on the mechanical properties of waste tire rubber concrete. *Constr. Build. Mater.* **2020**, *237*, 117651. [CrossRef]
20. Pham, T.M.; Davis, J.; Ha, N.S.; Pournasiri, E.; Shi, F.; Hao, H. Experimental investigation on dynamic properties of ultra-high-performance rubberized concrete (UHPRuC). *Constr. Build. Mater.* **2021**, *307*, 125104. [CrossRef]
21. Bahrami, H.; Mazaheri, H.; Bayat, A.; Parvari, A. Utilizing sugar factory lime waste and crumb rubber for sustainable Ultra-High-Performance Concrete. *Case Stud. Constr. Mater.* **2024**, *20*, e03395. [CrossRef]
22. Chen, G.; Zhuo, K.-X.; Luo, R.H.; Lai, H.M.; Cai, Y.J.; Xie, B.X.; Lin, J.X. Fracture behavior of environmentally friendly high-strength concrete using recycled rubber powder and steel fibers: Experiment and modeling. *Case Stud. Constr. Mater.* **2024**, *21*, e03501. [CrossRef]
23. Zhang, L.; Wang, H.; Wang, A.; Zhang, Q.; Li, Z.; Wang, X.; Huang, C.; Jivkov, A. Experimental study of marine ultra-high-performance concrete with coarse aggregate (UHPC-CA). *Case Stud. Constr. Mater.* **2025**, *22*, e04731. [CrossRef]
24. Li, W.; Yu, L.; Zhang, T. Quantitative analysis of grain size effect on tensile mechanical behavior of granite based on multi-level force chain networks. *Comp. Part. Mech.* **2024**, *11*, 2245–2266. [CrossRef]
25. Yu, R.; Spiesz, P.; Brouwers, H.J.H. Mix design and properties assessment of Ultra-High Performance Fiber Reinforced Concrete (UHPFRC). *Cem. Concr. Res.* **2014**, *56*, 29–39. [CrossRef]
26. Li, S.; Jensen, O.M.; Yu, Q. Influence of steel fiber content on the rate-dependent flexural performance of ultra-high performance concrete with coarse aggregates. *Constr. Build. Mater.* **2022**, *318*, 125935. [CrossRef]
27. Yu, R.; van Beers, L.; Spiesz, P.; Brouwers, H.J.H. Impact resistance of a sustainable Ultra-high performance fiber reinforced concrete (UHPFRC) under pendulum impact loadings. *Constr. Build. Mater.* **2016**, *107*, 203–215. [CrossRef]
28. *ASTM C143-20*; Standard Test Method for Slump of Hydraulic-Cement Concrete. ASTM International: West Conshohocken, PA, USA, 2020.
29. *ASTM C1611-18*; Standard Test Method for Slump Flow of Self-Consolidating Concrete. ASTM International: West Conshohocken, PA, USA, 2018.
30. *ASTM C39/C39M-21*; Standard Test Method for Compressive Strength of Cylindrical Concrete Specimens. ASTM International: West Conshohocken, PA, USA, 2021.
31. *ASTM C496/C496M-17*; Standard Test Method for Splitting Tensile Strength of Cylindrical Concrete Specimens. ASTM International: West Conshohocken, PA, USA, 2017.
32. *NT Build 492*; Concrete, Mortar, and Other Cement-Based Products: Chloride Migration. Nordic Innovation Centre: Oslo, Norway, 1999.

33. *ASTM C779/C779M-09*; Standard Test Method for Abrasion Resistance of Horizontal Concrete Surfaces. ASTM International: West Conshohocken, PA, USA, 2009.
34. Zhao, Y.; Duan, Y.; Zhu, L.; Wang, Y.; Jin, Z. Characterization of coarse aggregate morphology and its effect on rheological and mechanical properties of fresh concrete. *Constr. Build. Mater.* **2021**, *286*, 122940. [CrossRef]

Disclaimer/Publisher's Note: The statements, opinions and data contained in all publications are solely those of the individual author(s) and contributor(s) and not of MDPI and/or the editor(s). MDPI and/or the editor(s) disclaim responsibility for any injury to people or property resulting from any ideas, methods, instructions or products referred to in the content.